EURASIP Journal on Advances in Signal Processing

RESEARCH Open Access

A spectrum estimation approach for accurate heartbeat detection using Doppler radar based on combination of FTPR and TWV

Haipeng Pan[1,2], Yongyang Zou[1] and Minming Gu[1*]

*Correspondence: guminming@zstu.edu.cn

[1] School of Information Science and Engineering, Zhejiang Sci-Tech University, Hangzhou 310018, China
[2] Director of Automation Department, Zhejiang Sci-Tech University, Hangzhou 310018, China

Abstract

Non-contact heartbeat detection using Doppler radar is extremely valuable for remotely monitoring and medical diagnosis on special occasions. Nevertheless, fast and accurate heart rate (HR) detection endures several challenges due to influential respiration interference and insufficient frequency spectrum resolution. In this paper, a novel heartbeat detection method with a compact Doppler radar is employed to accurately estimate some indicators of HR and heart rate variability. Firstly, a multiresolution analysis approach based on maximal overlap discrete wavelet transform is introduced to accomplish the preliminary separation of respiration and heartbeat. Subsequently, a template matched filter algorithm is further implemented to maximize the enhancement of the concealed heartbeat component and retrieve the heartbeat signal. Eventually, a novel spectrum estimation method combining frequency–time phase regression with time-window-variation technology is proposed to evaluate the real-time HR. It solves serious dominant frequency estimation deviation and insufficient frequency spectrum resolution in short-period time windows. The accuracy and timeliness of our proposed method are validated by 6 sets of experimental data sampled at the actual office. As a result, the HR detection accuracy is up to 99.70% in different-period time windows of 10 s and 92.09% in 3s. In addition, the mean relative error of extracted beat-to-beat intervals in 3 s ranges from 0.76 to 1.02%.

Keywords: Doppler radar, Heart rate (HR), Frequency–time phase regression (FTPR), Time-window-variation (TWV)

1 Introduction

Vital signs detection is of great significance in daily health monitoring and clinical medical diagnosis. On the one hand, the frequency of the heartbeat reflects the basic health status [1, 2]. On the other hand, the rhythm and intensity of the heartbeat are significantly beneficial for the diagnosis of heart disease to a great extent [3]. Compared with traditionally contact ways such as electrocardiography (ECG) [4], photoplethysmography (PPG) [5], and wristband pulse oximeter [6], non-contact heartbeat detection based on Doppler radar has superiorities for some special occasions where contact electrodes are impractical or inconvenient, such as life detection during earthquake relief [7], infant monitoring [8], and fatigue detection [9].

© The Author(s) 2022. **Open Access** This article is licensed under a Creative Commons Attribution 4.0 International License, which permits use, sharing, adaptation, distribution and reproduction in any medium or format, as long as you give appropriate credit to the original author(s) and the source, provide a link to the Creative Commons licence, and indicate if changes were made. The images or other third party material in this article are included in the article's Creative Commons licence, unless indicated otherwise in a credit line to the material. If material is not included in the article's Creative Commons licence and your intended use is not permitted by statutory regulation or exceeds the permitted use, you will need to obtain permission directly from the copyright holder. To view a copy of this licence, visit http://creativecommons.org/licenses/by/4.0/.

As a kind of radar sensor, frequency-modulated-continuous-wave radar has been widely concerned with remotely monitoring vital signs such as respiration and heartbeat during the last decades [10–12]. So far, many quadrature demodulation methods have been presented one after another due to the widespread application of quadrature receiver architecture with I/Q channel demodulation [13]. The small-angle approximation [14] performs well only by presetting the target position. The complex signal demodulation [15] introduces harmonic interference and seriously reduces HR detection accuracy. Besides, the arctangent demodulation [16] is insensitive to the target position and harmonic interference but remains strong nonlinearity and discontinuity. Furthermore, the extended differentiate and cross-multiply [17] algorithm overcomes the shortcomings of phase wrapping and harmonic interference. Nevertheless, an error accumulation problem due to the discrete integration needs to be solved.

One of the challenges for heartbeat detection is accurately estimating HR under the strong interference of respiration and its harmonics. This is because the chest-wall displacements due to heartbeat (0.1–0.5 mm) are far smaller than those caused by respiration (1–12 mm). A succession of representative methods has been executed for cardiopulmonary signal separation and extraction to eliminate respiration interference, such as continuous wavelet transform (CWT) [18, 19], ensemble empirical mode decomposition (EEMD) [19, 20], singular spectrum analysis [21], and variational mode decomposition [22]. Although the effectiveness of these methods has been demonstrated for the separation and recovery of respiration and heartbeat, there are still some shortcomings. On the one hand, the above methods are remarkably susceptible to the signal-to-noise ratio. On the other hand, their computational cost is greatly increased. Recently, the capability and robustness of recovering the heartbeat signal based on the characteristic that matched filters can maximize the output signal-to-noise ratio have been substantiated in the presence of large-scale random body movements [23]. Furthermore, multiresolution analysis (MRA) proposed in [24] has been widely applied for fault detection [25], radar systems [26], and medical diagnosis [27]. In contrast, the MRA performance in vital signs research using Doppler radar is looking forward to being further validated.

Another challenge is the insufficient frequency spectrum resolution in short-period time windows. Sufficient frequency spectrum resolution can be achieved using long-period time windows of more than 10 s [20, 28, 29]. Nevertheless, the calculated HRV results will be the long-period averages in long-period time windows. In other words, the longer the time windows are, the more the losses of heartbeat details will be. Therefore, for HRV detection in frequency domain analysis, radar data processing in short-period time windows is required for fast HR acquisition. A time-window-variation (TWV) technique [30–32] is introduced to acquire the best time window and improve the HR accuracy in short-period time windows. Furthermore, the frequency–time phase regression (FTPR) [33, 34] can assess the HR robustly in low signal-to-noise ratio conditions and significantly advance the frequency spectrum resolution. Yet, a solution demands to be advised in response to serious dominant frequency estimation deviation in short-period time windows.

In this article, we present a fast and accurate approach for non-contact heartbeat detection using Doppler radar. We first demodulate the quadrature radar echo signal

to calculate the chest-wall displacement signal. Then, the heartbeat signal is accurately separated and retrieved from the chest-wall displacement signal. Furthermore, an effective and robust spectrum estimation method is employed to estimate the real-time HR. Finally, human subject experiments in an actual office environment will further verify the consistency of HR and BBIs between radar and ECG.

2 System architecture of Doppler radar

The fundamental principle of vital signs detection using continuous wave Doppler radar is to capture the frequency shift caused by the chest-wall displacement due to respiration and heartbeat. The vital signs detection system using 77 GHz millimeter-wave radar is shown in Fig. 1. Except for the PC and the subjects, the rest are all integrated into the radar development hardware platform to collect radar data containing the chest-wall movement information. The radar data are uploaded to the PC through the serial port for subsequent algorithm processing. In this paper, the millimeter-wave radar positioned in front of the subject at a distance of d_0 is employed to extract the chest-wall displacement signal $x(t)$. The radar transmitted signal can be expressed as

$$T(t) = \cos\left[2\pi ft + \varphi(t)\right] \tag{1}$$

where f and $\varphi(t)$ are carrier frequency and initial phase, respectively. Firstly, $T(t)$ is transmitted toward the subject from the transmitter (Tx). Then, the phase of $T(t)$ is modulated by the chest-wall displacement signal $x(t)$ and the reflected signal is generated. The reflected signal captured at the radar receiver (Rx) can be depicted as

$$R(t) \approx \cos\left[2\pi ft - \frac{4\pi d_0}{\lambda} - \frac{4\pi x(t)}{\lambda} + \varphi\left(t - \frac{2d_0}{c}\right)\right] \tag{2}$$

where c denotes the velocity of radio wave, and $\lambda = c/f$ denotes the wavelength of carrier. Generally, the reflected signal can be approximated as a $T(t)$ after phase modulation, with a time delayed of $2d_0/c$. After passing through the low-noise amplifier (LNA) at the front end of Rx, the baseband signal $B(t)$ can be represented as

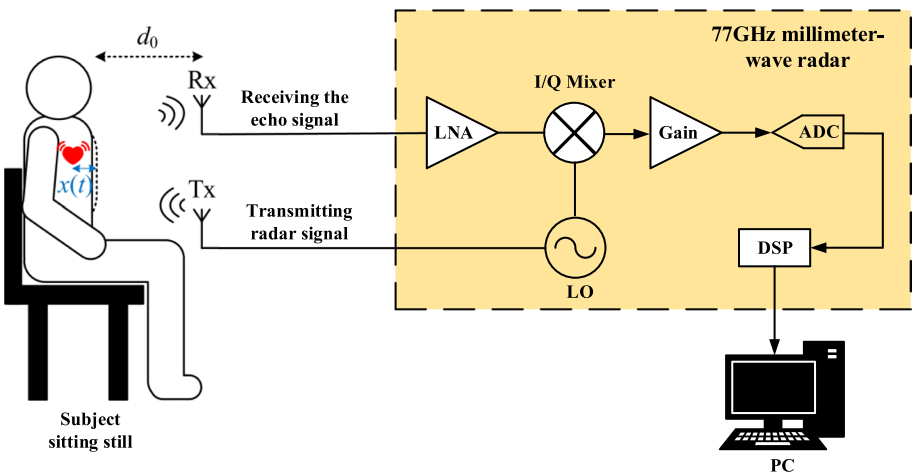

Fig. 1 77 GHz millimeter-wave radar system for heartbeat detection

$$B(t) = T(t) - R(t) = \cos\left[\theta + \frac{4\pi x(t)}{\lambda} + \Delta\varphi(t)\right] \tag{3}$$

where $\theta = 4\pi d_0/\lambda + \theta_0$ is the constant phase related to the initial phase shift θ_0 and the distance d_0, and the residual phase noise is simplified as $\Delta\varphi(t) = \varphi(t) - \varphi\left(t - 2d_0/c\right)$. Subsequently, the baseband signal $B(t)$ is demodulated by the quadrature mixer (I/Q Mixer), and the in-phase and quadrature signals are expressed as, respectively,

$$I(t) = \cos\left[\theta + \frac{4\pi x(t)}{\lambda} + \Delta\varphi(t)\right] \tag{4}$$

$$Q(t) = \sin\left[\theta + \frac{4\pi x(t)}{\lambda} + \Delta\varphi(t)\right] \tag{5}$$

Finally, the analog baseband signal is converted into a digital signal through A/D. The radar digital signal is processed by the DSP hardware module, and the subjects' chest-wall movement data are output and uploaded to PC through the serial port.

3 Proposed method

To realize accurate heartbeat estimation with Doppler radar in a complex environment, a concrete implementation scheme of radar data processing is fulfilled, mainly consisting of four parts: quadrature signal demodulation, signal preprocessing, cardiopulmonary signal separation and extraction, and heartbeat spectrum estimation. The proposed algorithm flowchart is presented in Fig. 2, where "Radar Raw Signal" means the data uploaded by the

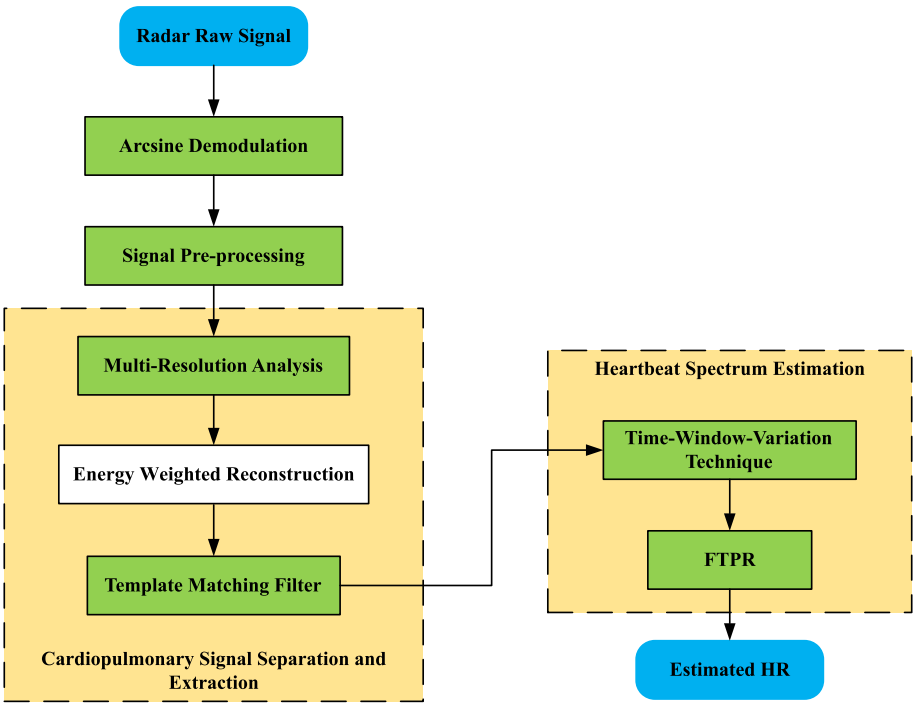

Fig. 2 Flowchart of the proposed HR estimation framework

radar development platform to the PC through the serial port. The remaining algorithm processing parts in the block diagram are all implemented on the PC side.

3.1 Quadrature signal demodulation

In this paper, we introduce the arcsine demodulation algorithm [35] into demodulating the quadrature signal. Due to discarding the arctangent's conventional method, phase wrapping and error accumulation problems can be avoided for the Doppler radar system with a low sampling rate. According to the above principle of vital signs detection, by discretizing the parameters t, the demodulated chest-wall displacement signal can be expressed as

$$x[n] = \frac{\lambda}{4\pi}\Phi[0] + \frac{\lambda}{4\pi}\sum_{k=2}^{n}\frac{I[k-1]Q[k] - I[k]Q[k-1]}{\sqrt{I[k-1]^2 + Q[k-1]^2}\cdot\sqrt{I[k]^2 + Q[k]^2}} \tag{6}$$

where k is the k-th sampled data of radar raw signal, λ is the wavelength of Doppler radar, $\Phi[0]$ is the initial phase, $I[k]$ and $Q[k]$ are the in-phase and quadrature signal of baseband, respectively, and $x[n]$ is the chest-wall displacement signal.

3.2 Signal preprocessing

Vital signs are completely overwhelmed by environmental noise. Signal preprocessing is implemented to remove background noise, eliminate polynomial trends, and enhance vital signs.

3.2.1 Clutter suppression

Assuming that the propagation environment within the radar measurement range is static, except for the subject's chest-wall motion, the constant features of stationary scatterers can be captured by averaging the chest-wall displacement data. Then, the background clutter can be removed by subtracting the average. In addition, the amplitude instability of the transmitting unit caused by thermal noise and time drift will result in a polynomial trend of the chest-wall displacement signal [36]. Because of a severe polynomial trend, the low-frequency components will distort or even drown the dominant frequency. Hence, it is necessary to eliminate the polynomial trend by subtracting the best fit line from the original chest-wall displacement.

3.2.2 Differential enhancement

Differentiating the chest-wall displacement signal can significantly enhance the high-frequency components in the displacement signal, namely the heartbeat and harmonic frequencies. In [37], the heart-to-respiration ratio increased by more than 16 times after first-order differential processing, validating the effectiveness of differential enhancement for weak heartbeat components. For the chest-wall displacement $\widetilde{x}[n]$ after clutter suppression, its first-order differential can be approximately expressed as

$$\widetilde{x}'[n] \approx \left[0\ \widetilde{x}_2 - \widetilde{x}_1\ \widetilde{x}_3 - \widetilde{x}_2\ \cdots\ \widetilde{x}_N - \widetilde{x}_{N-1}\right] \tag{7}$$

3.3 Cardiopulmonary signal separation and extraction

The next work is followed by signal preprocessing to accurately separate and extract the heartbeat signal under the influential interference of respiration and its harmonics.

3.3.1 MRA algorithm

Multiresolution analysis (MRA) establishes the connection between wavelet transform and digital filter. Based on this theory, a MRA approach based on MODWT is employed to decompose the preprocessing chest-wall displacement signal in multiple frequency bands and achieve the preliminary separation of heartbeat and respiration signals in this paper.

Wavelet transform is essentially a multiscale analysis that is implemented by scale and shift operations of a mother wavelet $\psi(t)$. For any function $f(t) \in L^2(R)$, the central frequency $\psi(t)$ of the mother wavelet is recorded as f_0; then, $f = f_0/a$, and the time–frequency form of wavelet transform can be depicted as follows

$$\mathrm{WT}_f(a,b) = \sqrt{\left|\frac{f}{f_0}\right|} \int_R f(t)\psi^*\left(\frac{f}{f_0}(t-b)\right)\mathrm{d}t \tag{8}$$

where a is a scale factor corresponding to frequency information, and b is a shift factor relating to space-time information. By setting the scale parameter a to change the shape of the window, it is possible to provide good time resolution for fast events such as heartbeat and excellent frequency resolution for slower events such as respiration, which is the multiresolution characteristic of the wavelet transform.

However, the continuous wavelet transform basis function $\psi_{a,b}(t)$ has a large computational redundancy for fast HR detection. Transformed into discrete wavelet transform by discretizing the parameters a and b, the calculation efficiency is exceedingly advanced. Therefore, set $a = a_0^i$, $b = jb_0a_0^i$, then the discrete wavelet can then be expressed as

$$\psi_{i,j}(t) = a_0^{-i/2}\psi\left(\frac{t - jb_0a_0^i}{a_0^i}\right) = a_0^{-i/2}\psi\left(a_0^{-i}t - jb_0\right) \tag{9}$$

Set $a_0 = 2$, $b_0 = 1$, it can be reduced to binary wavelet, expressed as

$$\psi_{i,j}(t) = 2^{-i/2}\psi(2^{-i}t - j) \tag{10}$$

Unlike traditional Fourier transform, wavelet transform has wavelet basis functions, such as Haar wavelet, Daubechies wavelet, Morlet wavelet, Symlet wavelet, and Coiflet wavelet. In this paper, the Coiflet wavelet is chosen as the mother wavelet according to the characteristics of the heartbeat signal for three reasons. Firstly, the wavelet function and scale function of the Coiflet wavelet have good symmetry, which can effectively avoid phase distortion. Secondly, the Coiflet wavelet function has a suitable tightly supported length and decays rapidly outside the effective supporting area. Finally, the shape of the Coiflet wavelet is similar to that of the heartbeat signal. The scaling function and wavelet function of the Coiflet5 wavelet are shown in Fig. 3, respectively.

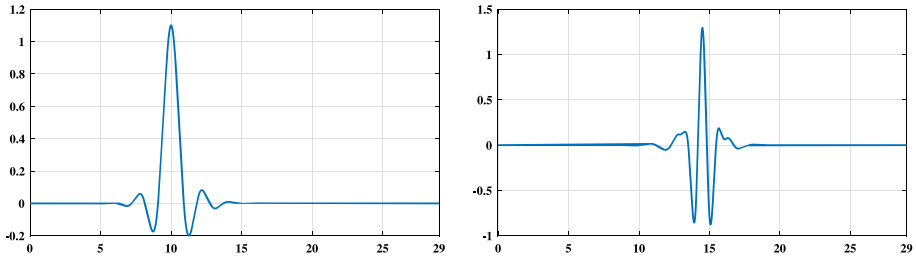

(a) scale function (b) wavelet function

Fig. 3 The function of the Coiflet5 wavelet

In this paper, the Coiflet wavelet is selected as the mother wavelet of the discrete wavelet transform, the vanishing moment order is selected as 5 order, and the decomposition layers number is 6 layers. The MODWT is implemented on the preprocessed chest-wall displacement signal $\widetilde{x}'[n]$, and the calculated wavelet transform matrix is denoted as $\mathrm{WT}_{(L+1)\times N}$, where L is the number of decomposition layers and N is the number of samples of the displacement signal. Then, the Coiflet5 wavelet is used to perform MRA on $\mathrm{WT}_{(L+1)\times N}$, and the calculated MRA matrix is denoted as $\mathrm{WT}_{\mathrm{mra}}$, whose different rows correspond to the MRA results at different scales.

Since HR typically varies from 0.8 to 2 Hz, it is supposed that the frequency range corresponds to the range from the k-th line to the l-th line of $\mathrm{WT}_{\mathrm{mra}}$. Besides, the energy distribution characteristics of wavelet coefficients are closely related to the frequency characteristics of the signal. Therefore, weighted reconstruction of different frequency bands based on the energy ratio can highlight the heartbeat's fundamental frequency component. The energy of each scale can be depicted as

$$E^{(i)} = \sum_{n=1}^{N} \left[\mathrm{WT}_{\mathrm{mra}}^{(i)}[n]\right]^2 \tag{11}$$

where i denotes the i-th layer of the wavelet decomposition, $i = 1, 2, \ldots, L+1$. $\mathrm{WT}_{\mathrm{mra}}^{(i)}[n]$ denotes the n-th wavelet coefficient of the i-th row. $E^{(i)}$ denotes the energy of the i-th layer. Then, the energy-weighted reconstructed heartbeat signal can be expressed as

$$x_{\mathrm{mra}}[n] = \sum_{i=k}^{l} \left(\frac{E^{(i)}}{\sum_{i=k}^{l} E^{(i)}} \right) \mathrm{WT}_{\mathrm{mra}}^{(i)} \tag{12}$$

where $\mathrm{WT}_{\mathrm{mra}}^{(i)}$ represents the wavelet coefficients matrix of the i-th row, and $x_{\mathrm{mra}}[n]$ represents the chest-wall displacement signal after preliminary separation and reconstruction using the MRA algorithm.

3.3.2 TMF algorithm

In the field of signal processing, a matched filter is an optimal filter, and its optimal criterion is the maximum signal-to-noise ratio of the output signal [38]. As for radar systems, matched filters have been universally applied in impulse radars, where the transmitted signal is adopted as the template signal [39]. Still, matched filters are rarely used in the field of vital signs detection with Doppler radar. Template matched filters, through

convolution operation between the input signal and the "template signal," can maximize the recovery of the signal similar to the template signal hidden in the original input signal.

The key to the template matching filter is the selection of the template signal. In [23], the low-speed segment signal is directly selected as the template signal. Then, the body motion in the template signal is removed by polynomial fitting to obtain the heartbeat template signal. The method difficulties lie in the choice of the polynomial fitting order and low extraction accuracy. Therefore, a template selection way is proposed to avoid respiration interference in this paper. During the experiment, the subject is requested to hold his respiration for a few seconds to derive the chest-wall displacement signal caused by only the heartbeat as the template signal. Subsequently, a convolution operation between the energy-reconstructed displacement signal and the "template signal" is carried out in the time domain. Then, the signal after template matching filter can be calculated by convolving $x_{\mathrm{mra}}[n]$ with a conjugated, time-reversed version of the template signal $h[n]$, that is,

$$x_h[n] = x_{\mathrm{mra}}[n] * h^*[-n] \tag{13}$$

To intuitively illustrate our proposed separation and extraction algorithm, the discrepancy is investigated by examining the chest-wall displacement waveforms' visualization and corresponding spectra, as illustrated in Fig. 4. The chest-wall displacement waveforms of different processing stages are shown in Fig. 4 on the left, and their corresponding spectra are shown in Fig. 4 on the right. Comparing Fig. 4a, b with Fig. 4c, d, it can be easily seen that the background clutter is effectively suppressed by the preprocessing, and the chest-wall displacement signal due to respiration and heartbeat is significantly enhanced. As displayed in Fig. 4e and f, the displacement amplitude decreased approximately 5 times and the respiration's frequency fundamental frequency component is

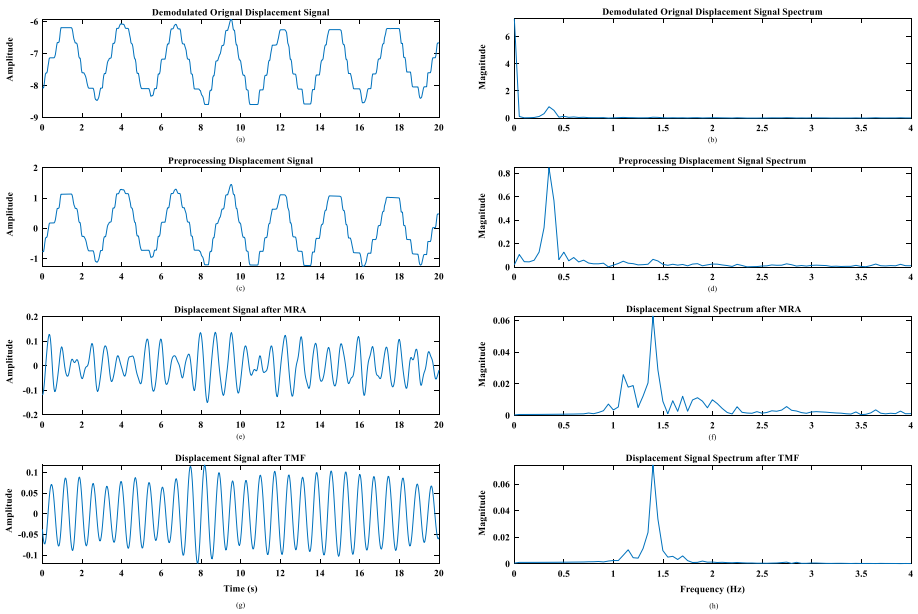

Fig. 4 A contrast of the chest-wall displacement waveforms and corresponding spectra

eliminated, showing that the preliminary separation of respiration and heartbeat is fulfilled by applying the MRA. Furthermore, as presented in Fig. 4g and h, the displacement signal has a powerful periodicity and its dominant spectrum peak is exceedingly significant, demonstrating that the TMF can recover the heartbeat signal concealed in the respiration signal.

3.4 Heartbeat spectrum estimation

The HR detection using Doppler radar is essentially a frequency estimation problem, and the frequency resolution determines the HR estimation accuracy. For a short-period time window of less than 5s, it is difficult for the traditional FFT to estimate HR quickly and accurately because of the lack of frequency resolution.

3.4.1 FTPR algorithm

Based on the fact that the phase varies linearly with time when the signal exists a dominant frequency [33], the FTPR algorithm converts the traditional frequency domain peak detection into a linear regression fitting of the phase and time in the time domain, and the slope of the phase is proportional to the dominant frequency of the signal. In [33], taking the time window $T = 10$ s as an example, the frequency resolution of FFT is 0.1 Hz, but that of FTPR is 0.01 Hz. Owing to the increased frequency resolution, HR detection accuracy is greatly promoted. Additionally, the heartbeat signal clearly has a dominant frequency, which is the heartbeat frequency. Consequently, the FTPR is an ideal choice. The specific steps of the FTPR for HR detection are as follows

1. The heartbeat signal $x_h[n]$ is windowed in the time domain, denoted as $x_{h\_win}[n]$. Windowing in the time domain can alleviate the spectral leakage of the signal.
2. The FFT is applied to the signal $x_{h\_win}[n]$ to acquire its spectrum, and the spectrum peak is determined. Preserved the frequency corresponding to the peak and its adjacent frequency, the rest of the spectrum is discarded to obtain a reconstructed spectrum
3. The inverse FFT of the reconstructed spectrum calculates a complex signal $x_{h\_rec}[n]$, where the real and imaginary parts are recorded as $I_h[n]$ and $Q_h[n]$, respectively. Referring to Eq. 6, the phase $\varphi_h[n]$ can be calculated by applying demodulation technology to $x_{h\_rec}[n]$.

$$\varphi_h[n] = \sum_{k=2}^{n} \frac{I_h[k-1]Q_h[k] - I_h[k]Q_h[k-1]}{\sqrt{I_h[k-1]^2 + Q_h[k-1]^2} \cdot \sqrt{I_h[k]^2 + Q_h[k]^2}} \tag{14}$$

4. The desired frequency can be calculated as follows

$$f_h = \text{Slope}[\varphi_h[n]]/2\pi \tag{15}$$

3.4.2 FTPR-TWV algorithm

However, the dominant peak of the heartbeat spectrum will seriously deviate from the true heartbeat frequency in short-period time windows. The reasons are as follows: First, there is still residual harmonic noise in the extracted heartbeat signal. Second,

the true heartbeat frequency is not an integer multiple of the frequency resolution due to insufficient frequency resolution. Aiming at the above shortcomings, a novel spectrum estimation method combining FTPR with TWV is proposed in this paper.

For a time window of *T*s, the frequency resolution Δf is calculated as $\Delta f = 1/T$. To measure the HR accurately, one of the following conditions or both should be satisfied: (a) $\Delta f \ll \mathrm{HR}$, (b) $\mathrm{HR} = k\Delta f$, where k is an integer number. Obviously, the detection accuracy can be satisfied by increasing the length of the time window, but the performance of the real-time detection is greatly reduced. In addition, for a periodic signal with a frequency of f, if the length of the time window is not an integer multiple of the period or in other words, $f \neq m\Delta f$, the sideband spurs or the harmonics will come out after the FFT, and the fundamental frequency energy will be degraded [30]. The closer the ratio is to an integer multiple, the smaller the fundamental frequency energy leakage is. The specific steps of "Acquire the best time window" are as follows.

1. Select the time window of *Ts* from the heartbeat signal extracted by cardiopulmonary signal separation and extraction as the original time window
2. Sampling in the range of $[T - \Delta t, T + \Delta t]$ at a time interval of $S = 1/f_s$, a series of time windows with different lengths are generated, and a series of different frequency resolutions are obtained, where f_s is the sampling frequency, and $\Delta t < 0.1T$. (The HR can be regarded as constant when Δt is small.)
3. Use FFT to calculate the heartbeat spectrum corresponding to each time window and draw all the heartbeat spectrograms in the same spectrogram to obtain the spectrum combination. This is the concept of "Spectrum combination."
4. Based on the fundamental frequency spur theory proposed above, by looking for the maximum value of the spectrum peak in the "Spectrum combination," the integer multiple of the frequency resolution of the time window corresponding to the maximum value is closest to the HR. This is the concept of "the best time window" proposed in this paper.

According to above steps, the number of time windows is jointly determined by the time interval S and the time variation Δt and has nothing to do with the original window size T. The more time windows there are, the more frequency resolutions are obtained, the closer the integer multiple of the frequency resolution of the best time window is to the HR, and the higher the detection accuracy. However, the computational cost will increase significantly, and trade-offs are required in the practical applications. In this paper, the time interval as $S = 1/f_s$ is selected.

An intuitive superiority of the combined spectrum of TWV is visualized in Fig. 5. As an example in the time window of $T = 3$ s and sampling frequency of $f_s = 32$ Hz, a series of different time windows are generated. As shown in Fig. 5, the spectrum peak of the 3s time window is 0.215, corresponding to a frequency of 1.333 Hz. However, the maximum peak in the combined spectrum is 0.223, corresponding to a time window of 3.179 s and a frequency of 1.255 Hz. Furthermore, because the reference frequency measured by ECG is 1.258 Hz, the time window of 3.179 s is unmistakably the best. Based on the above visual analysis, the severe dominant frequency estimation deviation can be avoided by introducing the TWV.

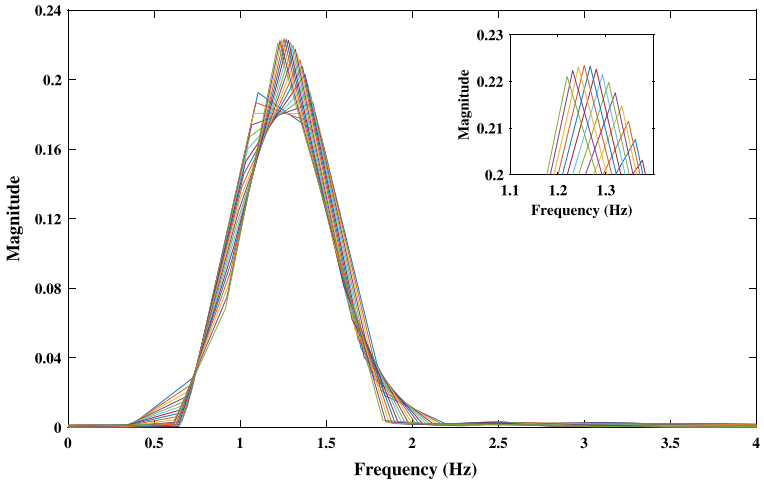

Fig. 5 An intuitive superiority of the combined spectra of TWV

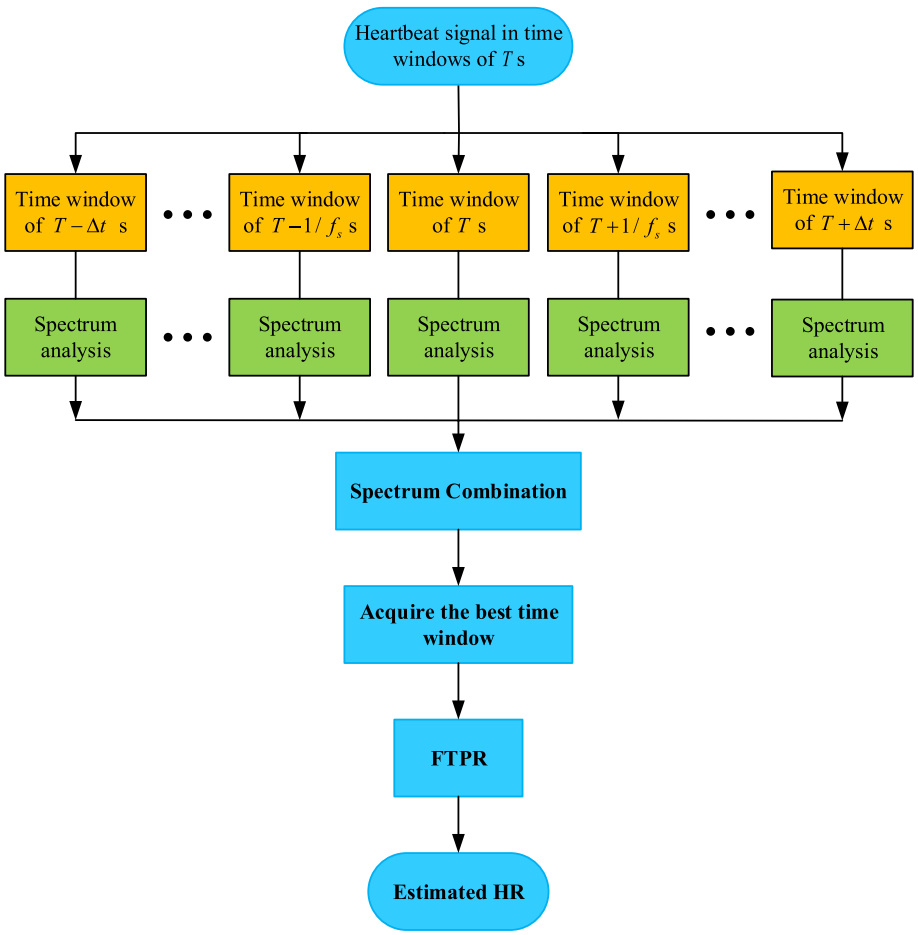

Fig. 6 Flowchart of FTPR-TWV framework

The FTPR-TWV algorithm is illustrated by conducting visual analysis of the specific implementation, as manifested in Fig. 6. This flowchart shows more details of the "Heartbeat Spectrum Estimation" part in Fig. 2. Following the TMF, the samples of the extracted heartbeat signal in the initial time window of T s are selected as input data, and a series of different-period time windows are generated by varying the time window size at a time interval $1/f_s$ from $T - \Delta t$ to $T + \Delta t$, where $\Delta t < 0.1T$. Afterward, a series of the spectra can be acquired by applying FFT to each time window, combining all the spectra into a spectrum. By searching for the largest spectral peak in the combined spectrum, the time window corresponding to this peak is the best. Finally, the HR, closest to the true HR, can be estimated using the FTPR algorithm on the sampled data of the best time window.

4 Experimental results and discussion

To verify the reliability of the heartbeat detection algorithm proposed in this paper, many experimental datasets are measured under different experimental conditions. Moreover, effective evaluation indicators are adopted to evaluate the performance of the proposed method.

4.1 Experimental conditions and parameters

The experiments are completed in an actual office environment, as exhibited in Fig. 7. The HR reference data in this experiment are measured by the traditional contact ECG acquisition module (the lower right corner in Fig. 7). ECG electrodes are attached to the subject's chest near the heart, and the sampling frequency is set to 500 Hz. The subject's ECG data are uploaded to the PC through serial port 2. The subject's ECG data are uploaded to the PC through serial port 2. IWR1443Boost (the upper right corner in Fig. 7) radar platform designed by Texas Instruments is adopted, and the relevant experimental parameters of the Doppler radar are displayed in Table 1. The subjects' chest-wall movement data are uploaded to the PC through data serial port 1. The actual office environment makes the experimental data closer to the data in the practical application.

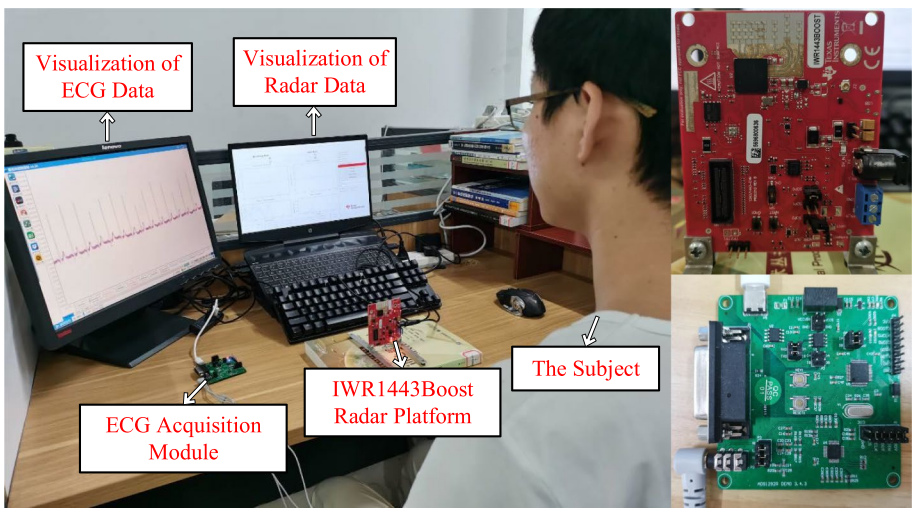

Fig. 7 Photographs of the experimental setup in an actual office environment

Table 1 Experimental parameters

Parameters	Value
Bandwidth	4 GHz
Starting frequency	77 GHz
Fast time axis sampling	2 MHz
Slow time axis sampling	32 Hz
Experimental distance	50 cm
Subjects' activities	Sitting still
Measurement duration	2 min
Time window period	3 s
	10 s

As for each experiment, 2 min of data were recorded from the subject 0.5 m away from the Doppler radar, sitting still in front of the radar and breathing normally. The 6 sets of experimental data are the measurement results of two male subjects at different times in the morning, middle and evening. Each set of data contains a 2 min measurement signal. A total of two subjects participate in the vital sign detection experiments.

Besides, the time resolution and frequency resolution need to be compromised in practical applications. Generally speaking, the shorter the time window is, the more heartbeat details can be presented, yet the lower the frequency resolution will be, the worse HR detection accuracy will be. Therefore, to prove the universality of the proposed algorithm for different occasions, two different-period time windows, respectively, 3 s and 10 s, are chosen for the HR detection.

4.2 Experimental results evaluation

Compared with a band-pass filter (BPF) and EEMD-based algorithm to verify the superiority of the proposed cardiopulmonary signal separation and extraction algorithm, a synchronized data segment of 10 s from the sixth set of data is picked to present the extracted heartbeat signal clearly, respectively. Additionally, the BPF is set as a 10-order Butterworth filter with a passband range from 1 to 3 Hz, and the matched template signal is decided by holding respiration for 5 s in sitting still.

As illustrated in Fig. 8, the blue line represents the reference ECG signal. The red line represents the heartbeat waveform extracted by the incorporation of MRA and TMF. The black line represents the heartbeat waveform extracted by the association of BPF and EEMD. In contrast to the mode mixing of the heartbeat waveform extracted by BPF and EEMD, the heartbeat waveform extracted by MRA and TMF is extremely periodic. Besides, the troughs of the waveform extracted by MRA and TMF basically correspond to the R peak of the ECG signal, indicating the similarity of the real-time HR between radar and ECG.

Based on the superiority of the heartbeat signal extraction algorithm mentioned above, comparing the performances of FFT-TWV, FTPR, and FTPR-TWV algorithms in HR detection, the development of our proposed spectrum estimation method will be evaluated by analyzing the heartbeat parameters of HR and HRV.

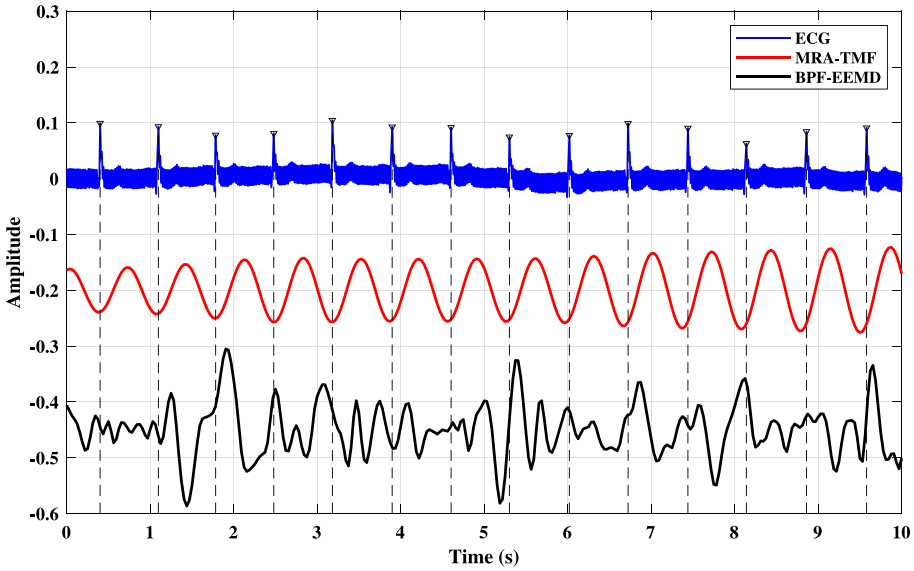

Fig. 8 An example showing the comparison of extracted heartbeat signals by different algorithms

4.2.1 HR analysis

Heart rate (HR) refers to the average number of heartbeats per minute, often used as a basic indicator of health monitoring. HR accuracy is defined as the percentage of time where HR detected by Doppler radar is within $\pm 2\%$ the deviation of the reference HR detected by ECG, which is also used as an HR indicator in this paper.

To visually demonstrate the performance advantages of our proposed algorithm in different-period time windows, the HR estimation results of different algorithms at different time windows from dataset 6 are exhibited in Fig. 9 as a reference from ECG. As shown in Fig. 9a, the HR accuracies of the three algorithms within the deviation are about 96%. However, two severe deviation points in the HR curve of the FTPR remain to be discovered due to the dominant frequency divergence, and the losses of the heartbeat details are grave. As depicted in Fig. 9b, the HR accuracy of the FTPR algorithm is only 43.22%, resulting from the severe dominant frequency estimation deviation in short-period time windows. Thus, the TWV algorithm is introduced into the FTPR algorithm to avoid the problem, and the best time window is determined.

As a result, the HR accuracy of the FTPR-TWV is up to 94.07%. Furthermore, the high agreement can be accomplished for the FTPR-TWV algorithm in tracking the large HR mutation points and presenting the HR variety, supporting the accuracy and timeliness of our proposed algorithm.

In addition, an error evaluation index is utilized: The root-mean-squared error (RMSE) is calculated as

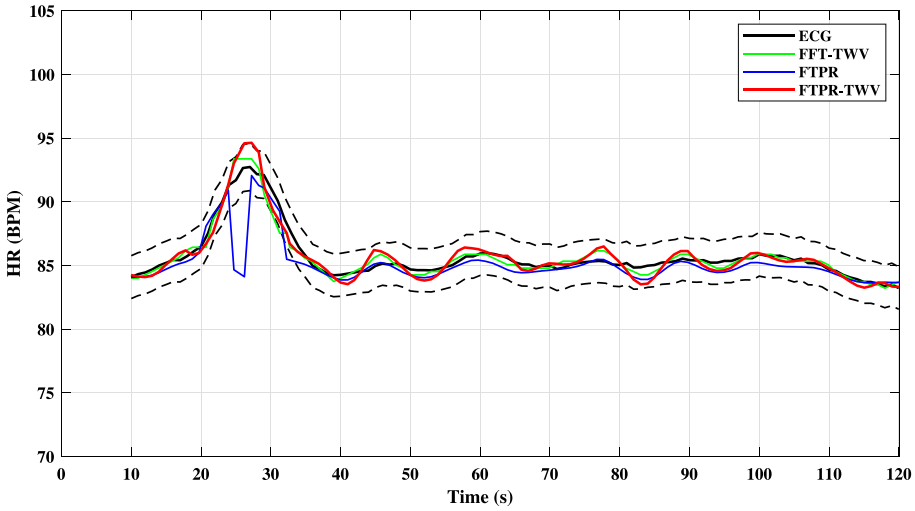

(a) $T = 10$ s

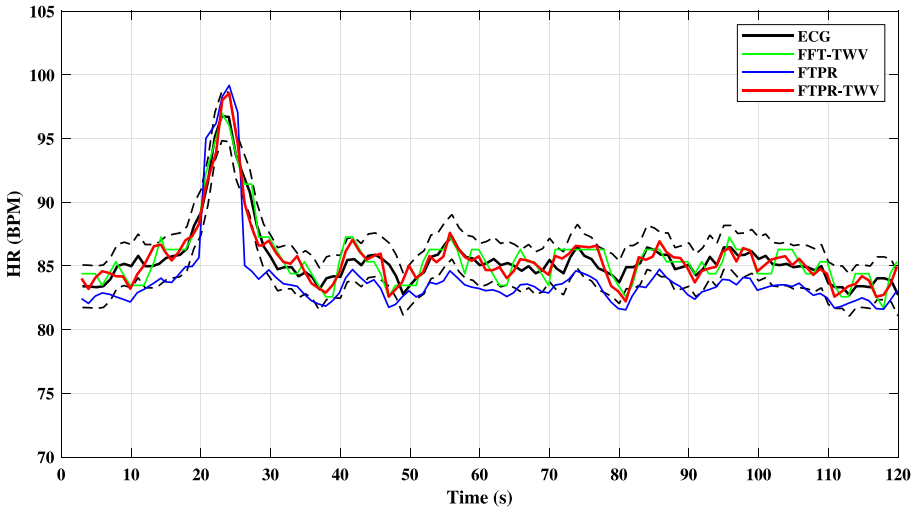

(b) $T = 3$ s

Fig. 9 An example showing the comparison of HR estimated of different algorithms from dataset 6

$$\mathrm{RMSE} = \sqrt{\frac{1}{N_{\mathrm{bpm}}} \sum_{i=1}^{N_{\mathrm{bpm}}} [\mathrm{BPM}_{\mathrm{est}}(i) - \mathrm{BPM}_{\mathrm{ref}}(i)]^2} \tag{16}$$

where N_{bpm} denotes the calculated HR number in the observation, $\mathrm{BPM}_{\mathrm{est}}(i)$ denotes the i-th estimated HR from Doppler radar, and $\mathrm{BPM}_{\mathrm{ref}}(i)$ denotes the i-th estimated HR from ECG, in units of beats per minute (BPM).

Taking the estimated HR results in Table 2 into consideration, we can further assess the achievements of different algorithms. Table 2 is divided into two sub-tables of basic time window $T = 10$ s and $T = 3$ s. Each sub-table has 6 groups of experimental data, each group of data corresponds to the estimation results of three different algorithms, and each row corresponds to the results of different indicators of the

Table 2 HR estimation results analysis

Dataset	Algorithm	Avg.HR (BPM)		HR accuracy (%)	RMSE (BPM)
		Radar	ECG		
(a) $T = 10$ s					
1	FFT-TWV	74.95	74.84	100.00	0.71
	FTPR	74.88		92.79	0.98
	FTPR-TWV	74.80		100.00	0.50
2	FFT-TWV	74.65	74.73	99.10	0.57
	FTPR	74.46		99.10	0.81
	FTPR-TWV	74.73		100.00	0.35
3	FFT-TWV	72.15	72.21	100.00	0.42
	FTPR	72.10		100.00	0.48
	FTPR-TWV	72.19		100.00	0.49
4	FFT-TWV	75.15	75.08	99.10	0.69
	FTPR	75.27		93.69	1.04
	FTPR-TWV	75.09		100.00	0.57
5	FFT-TWV	80.81	80.94	100.00	0.56
	FTPR	80.78		100.00	0.95
	FTPR-TWV	80.84		100.00	0.47
6	FFT-TWV	85.61	85.68	98.20	0.54
	FTPR	85.11		96.40	1.22
	FTPR-TWV	85.64		98.20	0.67
(b) $T = 3$ s					
1	FFT-TWV	74.84	74.79	86.44	1.01
	FTPR	76.65		37.29	2.06
	FTPR-TWV	74.78		89.83	0.99
2	FFT-TWV	74.70	74.72	84.75	0.99
	FTPR	76.56		33.90	2.03
	FTPR-TWV	74.65		92.37	0.89
3	FFT-TWV	72.99	72.17	55.09	1.76
	FTPR	74.31		12.71	2.52
	FTPR-TWV	72.16		93.22	0.80
4	FFT-TWV	75.10	75.10	86.44	1.03
	FTPR	76.88		32.20	1.98
	FTPR-TWV	75.11		88.98	0.98
5	FFT-TWV	80.85	80.90	91.53	0.98
	FTPR	80.56		84.75	1.06
	FTPR-TWV	80.87		94.07	0.78
6	FFT-TWV	85.62	85.55	88.98	1.05
	FTPR	83.84		43.22	2.15
	FTPR-TWV	85.55		94.07	0.95

algorithm. As shown in Table 2(a), the HR accuracies of the three algorithms are all over 92.79%, especially the average HR accuracy of FTPR-TWV is 99.70%, which is in high agreement with the reference value. As illustrated in Table 2(b), the average HR accuracies of FFT-TWV, FTPR, and FTPR-TWV are 82.20%, 40.68%, and 92.09%, respectively. The HR accuracy of FTPR-TWV is significantly higher than the comparison algorithm. In addition, the average RMSE of the FTPR-TWV is 0.90 BPM, which

Table 3 Comparison of the HR measurements with different algorithms

	Algorithms	Published year	Length of time windows	Error (%)
[30]	FFT-TWV	2016	2–5 s	3.40
[31]	IZA-SLMS with TWV	2019	8 s	4.20
[32]	WT-based data-length-variation	2017	2–5 s	3.00
[33]	FTPR	2018	10 s	9.50
[40]	the scaling function of WT	2019	–	3.90
[41]	SE	2021	–	1.60
This work	FTPR-TWV	–	3 s	0.03

is less than that of the FFT-TWV, further verifying that more details of the short-period HR variety can be presented (Table 3).

Furthermore, the relative error mean error is used as an indicator to compare the algorithm performances in recent years.

$$\text{Error} = \frac{1}{N}\sum_{n=1}^{N}\frac{|\text{HR}_{\text{ref}} - \text{HR}_{\text{est}}|}{\text{HR}_{\text{ref}}} \tag{17}$$

4.2.2 HRV analysis

Heart rate variability (HRV) refers to the time interval between consecutive heartbeats, revealing the regularity of each heartbeat. HRV analysis is of great significance in the diagnosis and medicine of heart diseases. Different from determining the BBIs by detecting the time interval of adjacent heartbeats in the time domain, the HR detection method by searching for the interested frequency in the frequency domain is applied in this paper and [31], where the BBIs can be calculated by the HR estimation value BPM, in units of beats per minute.

$$\text{BBI}(i) = \frac{60}{\text{BPM}(i)} \times 1000, \quad i = 1, 2, \ldots, N_{\text{bbi}} \tag{18}$$

The mean relative error (MRE) is defined as

$$\text{MRE} = \frac{1}{N_{\text{bbi}}}\sum_{i=1}^{N_{\text{bbi}}}\frac{|\text{BBI}_{\text{est}}(i) - \text{BBI}_{\text{ref}}(i)|}{\text{BBI}}_{\text{ref}}(i) \tag{19}$$

The evaluation indicators of HRV analysis, including the standard deviation of normal-to-normal intervals (SDNN) and the root-mean-square successive difference of intervals (RMSSD), are defined as

$$\text{SDNN} = \sqrt{\frac{1}{N_{\text{bbi}}}\sum_{i=1}^{N_{bbi}}\left[\text{BBI}(i) - \frac{1}{N_{\text{bbi}}}\sum_{i=1}^{N_{\text{bbi}}}\text{BBI}(i)\right]^2} \tag{20}$$

$$\mathrm{RMSSD} = \sqrt{\frac{1}{N_{\mathrm{bbi}} - 1} \sum_{i=2}^{N_{\mathrm{bbi}}} [\mathrm{BBI}(i) - \mathrm{BBI}(i-1)]^2} \tag{21}$$

where N_{bbi} is the number of successive heartbeat intervals and represents the time interval between successive heartbeats. In addition, the Bland–Altman analysis [42] is often used in medical clinical research to assess the consistency of different parameters. This method is also adopted to evaluate the agreement of the BBIs from radar and ECG in this paper, where the Bias denotes the average difference, and SD denotes the standard deviation of the difference. The lower and upper 95% limits of agreement (95% LoA) are defined as

$$\begin{aligned} LoA\_L &= \mathrm{Bias} - 1.96\mathrm{SD} \\ LoA\_U &= \mathrm{Bias} + 1.96\mathrm{SD} \end{aligned} \tag{22}$$

The results of HRV analysis are visualized in Table 4. As shown in Table 4(a), the MRE of the FTPR-TWV ranges from 0.36 to 0.64%, and the bias and 95% limits of consistency are small, showing high agreement. In addition, the small RMSSD indicates that the BBIs have small fluctuations, implying the losses of the HR details. As presented in Table 4(b), the averages of the MRE by the algorithms of FFT-TWV, FTPR, and FTPR-TWV are 1.17%, 2.28%, and 0.91%, respectively. The mean differences of the HRV evaluation indicators between those algorithms and ECG are SDNNs (1.86 ms, 3.77 ms, 0.88 ms), and RMSSDs (4.05 ms, 5.35 ms, 2.84 ms), respectively. Compared with the performances by FTPR, the above errors by FTPR-TWV considerably decrease due to introduction of TWV into FTPR. Moreover, all bias magnitudes by FTPR-TWV are under 0.80 ms, further verifying the accuracy and timeliness of our proposed method in short-period time windows.

4.3 Discussion

As a result, accurate heartbeat estimation results have been implemented in short-period time windows of 3 s by using our proposed heartbeat detection algorithm. This method solves serious dominant frequency estimation deviation and insufficient frequency spectrum resolution in short-period time window. However, there are still many limitations as well as research topics to be further explored, mainly summarized as follows

1. The experimental test scenario in this paper is that the subject's chest is located directly in front of the radar for monitoring, which is relatively ideal and has limitations for wide applications in different fields. In practical applications, the human body may not be located at a certain angle or even back to the radar, resulting in a lower energy of the measured vital sign. Therefore, enhancement algorithm for vital sign components should be further studied.
2. Research on the methods of the heartbeat signal extraction in the presence of large body movements. The chest-wall motion caused by the heartbeat and respiration is much smaller than the large body movements, so it is difficult to extract vital signs from the radar echo signal in the presence of large body movements. As for heart-

Table 4 HRV estimation results analysis

Dataset	Algorithm	MRE (%)	SDNN (ms)		RMSSD (ms)		Bland–Altman (ms)		
			Radar	ECG	Radar	ECG	Bias	LoA_L	LoA_U
(a) $T = 10$ s									
1	FFT-TWV	0.85	11.03	7.52	5.03	2.08	− 1.17	− 16.04	13.70
	FTPR	1.18	14.54		6.13		− 0.27	− 20.97	20.42
	FTPR-TWV	0.50	8.69		1.93		0.47	− 10.04	10.99
2	FFT-TWV	0.59	9.71	7.86	5.24	2.48	0.86	− 10.94	12.67
	FTPR	1.01	13.87		4.66		3.02	− 13.12	19.16
	FTPR-TWV	0.36	8.21		1.89		− 0.03	− 7.30	7.24
3	FFT-TWV	0.47	11.09	10.81	2.58	2.14	0.65	− 8.79	10.09
	FTPR	0.52	7.27		1.27		1.14	− 9.52	11.80
	FTPR-TWV	0.55	12.12		2.21		0.24	− 10.92	11.41
4	FFT-TWV	0.77	10.45	6.67	4.21	1.72	− 0.70	− 15.15	13.75
	FTPR	1.28	14.88		4.07		− 1.82	− 23.35	19.71
	FTPR-TWV	0.64	8.98		2.51		− 0.10	− 12.06	11.86
5	FFT-TWV	0.57	8.64	5.62	4.00	1.39	1.23	− 8.55	11.01
	FTPR	1.10	12.95		5.04		1.64	− 15.21	18.50
	FTPR-TWV	0.45	8.17		2.02		1.01	− 7.30	9.33
6	FFT-TWV	0.42	15.00	15.20	4.08	3.16	0.52	− 7.60	8.64
	FTPR	0.72	12.81		8.45		4.60	− 11.86	21.05
	FTPR-TWV	0.58	16.56		4.67		0.38	− 9.87	10.64
(b) $T = 3$ s									
1	FFT-TWV	1.08	10.26	11.21	10.39	9.35	− 0.55	− 21.92	20.81
	FTPR	2.44	8.37		5.81		− 19.50	− 38.33	− 0.67
	FTPR-TWV	1.02	11.04		6.04		0.10	− 20.96	21.17
2	FFT-TWV	0.99	10.19	11.21	10.57	9.34	0.22	− 20.72	21.16
	FTPR	2.41	6.54		4.68		− 19.38	− 37.65	− 1.10
	FTPR-TWV	0.93	9.27		4.08		0.72	− 18.06	19.51
3	FFT-TWV	1.93	18.16	13.33	20.02	7.30	− 9.16	− 46.37	28.04
	FTPR	3.18	19.12		17.45		− 23.74	− 54.48	7.00
	FTPR-TWV	0.88	12.71		5.97		0.06	− 18.20	18.31
4	FFT-TWV	1.05	10.42	9.98	9.50	8.63	− 0.03	− 21.80	21.74
	FTPR	2.35	6.78		4.97		− 18.61	− 36.65	− 0.56
	FTPR-TWV	1.00	9.99		5.83		− 0.09	− 20.83	20.66
5	FFT-TWV	0.96	11.19	8.07	10.11	4.84	0.53	− 17.19	18.25
	FTPR	1.02	10.50		10.27		3.18	− 15.26	21.62
	FTPR-TWV	0.76	10.09		6.81		0.26	− 14.00	14.53
6	FFT-TWV	1.00	19.16	18.39	9.79	6.63	− 0.54	− 17.72	16.64
	FTPR	2.28	22.08		11.28		14.54	− 5.10	34.18
	FTPR-TWV	0.87	18.91		9.00		0.02	-15.21	15.26

beat detection in the presence of large body movements, more advanced algorithms will be required to exclude abnormal parameter values in the radar echo signal.

3. Research on the time domain characteristics of vital signs. The frequency domain analysis of vital signs can only obtain information such as heart rate and respiration rate in a specific time window. Nevertheless, as for clinical medical diagnosis, the time domain information of vital signs at each moment should be observed, which is a major focus of future research work.

5 Conclusion

In summary, the accuracy and timeliness of our proposed heartbeat detection method using Doppler radar are confirmed through theoretical analysis and human experiments. By employing the MRA and TMF methods, we can faithfully accomplish the cardiopulmonary signal separation and the hidden heartbeat signal recovery. Furthermore, a novel spectrum estimation approach can provide fast and accurate HR estimation and solve serious dominant frequency estimation deviation and insufficient frequency spectrum resolution in short-period time windows. Experimental results in short-period time windows of 3s demonstrate high accuracy and small average errors, including the HR detection accuracy of up to 92.09%, the BBIs' MRE of less than 1.05%, and the bias magnitudes of under 0.80 ms, verifying the presence of more HR characteristics and higher consistency between the radar and ECG. Therefore, the benefit of the accuracy and timeliness of our proposed method could be anticipated for non-contact vital signs detection research.

Abbreviations

mmWave	Millimeter-wave
HR	Heart rate
HRV	Heart rate variability
FTPR	Frequency–time phase regression
TWV	Time-window-variation
MRA	Multiresolution analysis
TMF	Template matched filter

Acknowledgements
This work is supported by the School of Mechanical Engineering and Automation, Zhejiang Sci-Tech University, Hangzhou, China.

Author contributions
The research and results of this specific publication are a long-term collaboration between the authors based on MIMO radar applications. All authors read and approved the final manuscript.

Funding
This work is supported by "Zhejiang Science Technology Department Public Service Technology Research Project" (Grant Number LGG19F030002).

Availability of data and materials
All data generated or analyzed during this study are included in this paper.

Declarations

Ethics approval and consent to participate
All procedures performed in this paper were in accordance with the ethical standards of research community.

Competing interests
The authors declare that they have no competing interests.

Received: 26 January 2022 Accepted: 10 July 2022
Published online: 26 July 2022

References

1. C. Li, V.M. Lubecke, O. Boric-Lubecke, J. Lin, A review on recent advances in doppler radar sensors for noncontact healthcare monitoring. IEEE Trans. Microw. Theory Tech. **61**(5), 2046–2060 (2013). https://doi.org/10.1109/TMTT.2013.2256924
2. D. Shao, Y. Yang, C. Liu, F. Tsow, H. Yu, N. Tao, Noncontact monitoring breathing pattern, exhalation flow rate and pulse transit time. IEEE Trans. Biomed. Eng. **61**(11), 2760–2767 (2014). https://doi.org/10.1109/TBME.2014.2327024
3. W. Xia, Y. Li, S. Dong, Radar-based high-accuracy cardiac activity sensing. IEEE Trans. Instrum. Meas. **70**, 1–13 (2021). https://doi.org/10.1109/TIM.2021.3050827

4. N. El-Sherif, P. Denes, R. Katz, R. Capone, L.B. Mitchell, M. Carlson, R. Reynolds-Haertle, Investigators**, C.A.S.T.-A.E.C.S., Definition of the best prediction criteria of the time domain signal-averaged electrocardiogram for serious arryhthmic events in thepostinfarction period. J. Am. Coll. Cardiol. **25**(4), 908–914 (1995)
5. Y. Sun, N. Thakor, Photoplethysmography revisited: from contact to noncontact, from point to imaging. IEEE Trans. Biomed. Eng. **63**(3), 463–477 (2016). https://doi.org/10.1109/TBME.2015.2476337
6. P.J. Soh, G.A.E. Vandenbosch, M. Mercuri, D.M.M.-P. Schreurs, Wearable wireless health monitoring: current developments, challenges, and future trends. IEEE Microw. Mag. **16**(4), 55–70 (2015). https://doi.org/10.1109/MMM.2015.2394021
7. K.-M. Chen, Y. Huang, J. Zhang, A. Norman, Microwave life-detection systems for searching human subjects under earthquake rubble or behind barrier. IEEE Trans. Biomed. Eng. **47**(1), 105–114 (2000). https://doi.org/10.1109/10.817625
8. N. Hafner, I. Mostafanezhad, V.M. Lubecke, O. Boric-Lubecke, A. Host-Madsen, Non-contact cardiopulmonary sensing with a baby monitor, in *2007 29th Annual International Conference of the IEEE Engineering in Medicine and Biology Society* (2007), pp. 2300–2302. https://doi.org/10.1109/IEMBS.2007.4352785
9. X. Gu, L. Zhang, Y. Xiao, H. Zhang, H. Hong, X. Zhu, Non-contact fatigue driving detection using CW Doppler radar, in *2018 IEEE MTT-S International Wireless Symposium (IWS)* (2018), pp. 1–3. https://doi.org/10.1109/IEEE-IWS.2018.8400971
10. M. Alizadeh, G. Shaker, S. Safavi-Naeini, Experimental study on the phase analysis of FMCW radar for vital signs detection, in *2019 13th European Conference on Antennas and Propagation (EuCAP)* (2019), pp. 1–4
11. S. Wang, A. Pohl, T. Jaeschke, M. Czaplik, M. Köny, S. Leonhardt, N. Pohl, A novel ultra-wideband 80 GHZ FMCW radar system for contactless monitoring of vital signs, in *2015 37th Annual International Conference of the IEEE Engineering in Medicine and Biology Society (EMBC)* (2015), pp. 4978–4981. https://doi.org/10.1109/EMBC.2015.7319509
12. G. Wang, C. Gu, T. Inoue, C. Li, A hybrid FMCW-interferometry radar for indoor precise positioning and versatile life activity monitoring. IEEE Trans. Microw. Theory Tech. **62**(11), 2812–2822 (2014). https://doi.org/10.1109/TMTT.2014.2358572
13. A.D. Droitcour, O. Boric-Lubecke, V.M. Lubecke, J. Lin, G.T.A. Kovacs, Range correlation and i/q performance benefits in single-chip silicon doppler radars for noncontact cardiopulmonary monitoring. IEEE Trans. Microw. Theory Tech. **52**(3), 838–848 (2004). https://doi.org/10.1109/TMTT.2004.823552
14. W. Massagram, V.M. Lubecke, A. HØst-Madsen, O. Boric-Lubecke, Assessment of heart rate variability and respiratory sinus arrhythmia via Doppler radar. IEEE Trans. Microw. Theory Techn. **57**(10), 2542–2549 (2009). https://doi.org/10.1109/TMTT.2009.2029716
15. C. Li, J. Lin, Complex signal demodulation and random body movement cancellation techniques for non-contact vital sign detection, in *2008 IEEE MTT-S International Microwave Symposium Digest* (2008), pp. 567–570. https://doi.org/10.1109/MWSYM.2008.4633229
16. T. Sakamoto, R. Imasaka, H. Taki, T. Sato, M. Yoshioka, K. Inoue, T. Fukuda, H. Sakai, Feature-based correlation and topological similarity for interbeat interval estimation using ultrawideband radar. IEEE Trans. Biomed. Eng. **63**(4), 747–757 (2016). https://doi.org/10.1109/TBME.2015.2470077
17. J. Wang, X. Wang, L. Chen, J. Huangfu, C. Li, L. Ran, Noncontact distance and amplitude-independent vibration measurement based on an extended DACM algorithm. IEEE Trans. Instrum. Meas. **63**(1), 145–153 (2014). https://doi.org/10.1109/TIM.2013.2277530
18. M. Mercuri, Y.-H. Liu, I. Lorato, T. Torfs, F. Wieringa, A. Bourdoux, C. Van Hoof, A direct phase-tracking doppler radar using wavelet independent component analysis for non-contact respiratory and heart rate monitoring. IEEE Trans. Biomed. Circuits Syst. **12**(3), 632–643 (2018). https://doi.org/10.1109/TBCAS.2018.2813013
19. W. Hu, Z. Zhao, Y. Wang, H. Zhang, F. Lin, Noncontact accurate measurement of cardiopulmonary activity using a compact quadrature doppler radar sensor. IEEE Trans. Biomed. Eng. **61**(3), 725–735 (2014). https://doi.org/10.1109/TBME.2013.2288319
20. C.-Y. Huang, G.-W. Fang, H.-R. Chuang, C.-L. Yang, Clutter-resistant vital sign detection using amplitude-based demodulation by EEMD-PCA-correlation algorithm for FMCW radar systems, in *2019 49th European Microwave Conference (EuMC)* (2019), pp. 928–931. https://doi.org/10.23919/EuMC.2019.8910730
21. Z. Zhang, Z. Pi, B. Liu, Troika: a general framework for heart rate monitoring using wrist-type photoplethysmographic signals during intensive physical exercise. IEEE Trans. Biomed. Eng. **62**(2), 522–531 (2015). https://doi.org/10.1109/TBME.2014.2359372
22. H. Shen, C. Xu, Y. Yang, L. Sun, Z. Cai, L. Bai, E. Clancy, X. Huang, Respiration and heartbeat rates measurement based on autocorrelation using IR-UWB radar. IEEE Trans. Circuits Syst. II Express Briefs **65**(10), 1470–1474 (2018). https://doi.org/10.1109/TCSII.2018.2860015
23. Q. Lv, L. Chen, K. An, J. Wang, H. Li, D. Ye, J. Huangfu, C. Li, L. Ran, Doppler vital signs detection in the presence of large-scale random body movements. IEEE Trans. Microw. Theory Tech. **66**(9), 4261–4270 (2018). https://doi.org/10.1109/TMTT.2018.2852625
24. B. Sendov, Adaptive wavelets and multiresolution analysis. C. R. l'Acad. Bulg. Sci. **53**(5), 5–21 (2000)
25. W. Li, A. Monti, F. Ponci, Fault detection and classification in medium voltage DC shipboard power systems with wavelets and artificial neural networks. IEEE Trans. Instrum. Meas. **63**(11), 2651–2665 (2014). https://doi.org/10.1109/TIM.2014.2313035
26. B.A. Raut, V. Louf, K. Gayatri, P. Murugavel, M. Konwar, T. Prabhakaran, A multiresolution technique for the classification of precipitation echoes in radar data. IEEE Trans. Geosci. Remote Sens. **58**(8), 5409–5415 (2020). https://doi.org/10.1109/TGRS.2020.2965649
27. J.-J. Qiu, J. Yin, W. Qian, J.-H. Liu, Z.-X. Huang, H.-P. Yu, L. Ji, X.-X. Zeng, A novel multiresolution-statistical texture analysis architecture: radiomics-aided diagnosis of PDAC based on plain CT images. IEEE Trans. Med. Imaging **40**(1), 12–25 (2021). https://doi.org/10.1109/TMI.2020.3021254
28. J. Tu, J. Lin, Respiration harmonics cancellation for accurate heart rate measurement in non-contact vital sign detection, in *2013 IEEE MTT-S International Microwave Symposium Digest (MTT)* (2013), pp. 1–3. https://doi.org/10.1109/MWSYM.2013.6697732

29. E. Schires, P. Georgiou, T.S. Lande, Vital sign monitoring through the back using an UWB impulse radar with body coupled antennas. IEEE Trans. Biomed. Circuits Syst. **12**(2), 292–302 (2018). https://doi.org/10.1109/TBCAS.2018.2799322
30. J. Tu, J. Lin, Fast acquisition of heart rate in noncontact vital sign radar measurement using time-window-variation technique. IEEE Trans. Instrum. Meas. **65**(1), 112–122 (2016). https://doi.org/10.1109/TIM.2015.2479103
31. C. Ye, K. Toyoda, T. Ohtsuki, A stochastic gradient approach for robust heartbeat detection with doppler radar using time-window-variation technique. IEEE Trans. Biomed. Eng. **66**(6), 1730–1741 (2019). https://doi.org/10.1109/TBME.2018.2878881
32. M. Li, J. Lin, Wavelet-transform-based data-length-variation technique for fast heart rate detection using 5.8-GHZ CW doppler radar. IEEE Trans. Microw. Theory Tech. **66**(1), 568–576 (2018). https://doi.org/10.1109/TMTT.2017.2730182
33. M. Nosrati, N. Tavassolian, High-accuracy heart rate variability monitoring using doppler radar based on Gaussian pulse train modeling and FTPR algorithm. IEEE Trans. Microw. Theory Tech. **66**(1), 556–567 (2018). https://doi.org/10.1109/TMTT.2017.2721407
34. M. Nosrati, N. Tavassolian, Accurate Doppler radar-based cardiopulmonary sensing using chest-wall acceleration. IEEE J. Electromagn. RF Microw. Med. Biol. **3**(1), 41–47 (2019). https://doi.org/10.1109/JERM.2018.2879452
35. T. Fan, C. Ma, Z. Gu, Q. Lv, J. Chen, D. Ye, J. Huangfu, Y. Sun, C. Li, L. Ran, Wireless hand gesture recognition based on continuous-wave Doppler radar sensors. IEEE Trans. Microw. Theory Tech. **64**(11), 4012–4020 (2016). https://doi.org/10.1109/TMTT.2016.2610427
36. D. Yang, Z. Zhu, B. Liang, Vital sign signal extraction method based on permutation entropy and EEMD algorithm for ultra-wideband radar. IEEE Access **7**, 178879–178890 (2019). https://doi.org/10.1109/ACCESS.2019.2958600
37. Y. Xiong, Z. Peng, C. Gu, S. Li, D. Wang, W. Zhang, Differential enhancement method for robust and accurate heart rate monitoring via microwave vital sign sensing. IEEE Trans. Instrum. Meas. **69**(9), 7108–7118 (2020). https://doi.org/10.1109/TIM.2020.2978347
38. R.T. Wakai, W.J. Lutter, Matched-filter template generation via spatial filtering: application to fetal biomagnetic recordings. IEEE Trans. Biomed. Eng. **49**(10), 1214–1217 (2002). https://doi.org/10.1109/TBME.2002.803523
39. J.R. Roman, M. Rangaswamy, D.W. Davis, Q. Zhang, B. Himed, J.H. Michels, Parametric adaptive matched filter for airborne radar applications. IEEE Trans. Aerosp. Electron. Syst. **36**(2), 677–692 (2000). https://doi.org/10.1109/7.845259
40. C.-H. Choi, J.-H. Park, H.-N. Lee, J.-R. Yang, Heartbeat detection using a doppler radar sensor based on the scaling function of wavelet transform. Microw. Opt. Technol. Lett. **61**(7), 1792–1796 (2019). https://doi.org/10.1002/mop.31823
41. S.H. Oh, S. Lee, S.M. Kim, J.H. Jeong, Development of a heart rate detection algorithm using a non-contact doppler radar via signal elimination. Biomed. Signal Process. Control **64**, 102314 (2021). https://doi.org/10.1016/j.bspc.2020.102314
42. J.M. Bland, D. Altman, Statistical methods for assessing agreement between two methods of clinical measurement. Lancet **327**(8476), 307–310 (1986). https://doi.org/10.1016/s0140-6736(86)90837-8

Publisher's Note

Springer Nature remains neutral with regard to jurisdictional claims in published maps and institutional affiliations.

Submit your manuscript to a SpringerOpen journal and benefit from:

- ► Convenient online submission
- ► Rigorous peer review
- ► Open access: articles freely available online
- ► High visibility within the field
- ► Retaining the copyright to your article

Submit your next manuscript at ► springeropen.com